PCCP

A new horizon for vibrational circular dichroism spectroscopy: a challenge for supramolecular chirality

Journal:	*Physical Chemistry Chemical Physics*
Manuscript ID	CP-PER-02-2020-000713.R2
Article Type:	Perspective
Date Submitted by the Author:	18-Mar-2020
Complete List of Authors:	Sato, Hisako; Ehime University, Department of Chemistry

ARTICLE

A new horizon for vibrational circular dichroism spectroscopy: a challenge for supramolecular chirality

Received 00th January 20xx,
Accepted 00th January 20xx

DOI: 10.1039/x0xx00000x

Hisako Sato[a,*]

Vibrational circular dichroism (VCD) spectroscopy is an extension of circular dichroism spectroscopy into the infrared and near-infrared regions where vibrational transitions occur in the ground electronic state of a molecule. The method offers the advantage of studying the chiroptical properties of a wide range of molecules in non-crystalline states. However, because of the smallness of the signals, one measurement requires several hours to yield reliable results. Accordingly, its targets were limited to a stable molecule in a solution. To overcome this difficulty, our group applied the VCD method to supramolecular systems. The work was launched based on the finding that the VCD signal remarkably enhances when low-molecular mass gelators form gels. By analysing a number of well-resolved VCD peaks, the detailed conformation of a component molecule was deduced. This provided a clue to elucidating the molecular organization in supramolecular architectures. Our final goal was to clarify the route from microscopic molecular chirality to supramolecular chirality. For this purpose, a time-step VCD measurement method was developed for the *in situ* monitoring of the progress of chirality amplification.

Introduction

Vibrational circular dichroism (VCD) spectroscopy is an extension of circular dichroism spectroscopy into the infrared region.[1–13] The method was initiated by Holzwarth *et al.* and developed by Nafie *et al.* in the 1970s,[8,9] and has been substantially assisted by the theoretical approach.[7] Since the VCD theory includes only the ground electronic state, it is considered more reliable and straightforward than the calculation of electronic circular dichroism (ECD) spectra.

A drawback of the VCD method is that the signal from an isolated single molecule is very small. The smallness of a signal is essential since a molecule is predicted to have no VCD activity within the scope of the Born–Oppenheimer approximation.[7] The intensity of a signal is expressed in terms of the dissymmetry factor denoted by the g-value, which is given by $g = \Delta A/A$, where A and ΔA are the absorbance and the difference in the absorbances of left- and right-handed circularly polarized lights (or $\Delta A = A_{left} - A_{right}$), respectively. The g-value for VCD ranges from 10^{-5} to 10^{-4} for an isolated chiral molecule in a solution, and is two or three-orders lower in magnitude than that for ECD (10^{-3}–10^{-2}).

The VCD spectra are usually measured for several hours through repeated scanning for 10^4–10^5 times. Thus, the main target is limited to the determination of the absolute configuration of stable chiral molecules in a solution. In this respect, the method is complementary to other spectroscopies such as single crystal X-ray or NMR analyses.

To overcome this limitation, improvements have been achieved by various approaches.[14–54] The enhancement of VCD signals is one such approach. In fact, the phenomena have been noted in several cases such as the aggregation of biomolecules in a solution or their crystalline states.[30–53] For example, the formation of insulin fibrils was studied by VCD spectroscopy in various conditions.[31–34] It is now in demand to determine the systems that can be studied in a more systematic way.[45,47] For instrumental improvement, a number of attempts have been made such as combining ATR-IR with VCD, using quantum cascade laser (QCL) as a light source, and introducing mapping systems with a micro-sampling accessory.[54–63] In spite of these efforts, construction of an instrument to measure the VCD spectrum of a sample with high optical density over a wide wavenumber range is yet to be realized.

Motivated by the above-mentioned research trends, our group applied the VCD method to samples other than organic molecules in solutions such as metal complexes,[64–75] gels,[76–89] liquid crystals,[90,91] molecular crystals,[92-98] and inorganic intercalation compounds.[99–101] Our aim was to clarify the mechanism of amplification of molecular chirality up to the supramolecular scale. We believe that the VCD method is unique in establishing the stereoregular arrangement of molecules over hundreds of nanometres. Moreover, the need to gain deep insight into this spectroscopy led to the synthesis of new compounds for specific purposes. The work was driven by the finding that the signal intensity increased tremendously when some chiral molecules formed a gel.[76,78,80] In comparison to the reported examples involving biomolecules such as

[a] *Department of Chemistry, Graduate School of Science and Engineering, Ehime University, Matsuyama 790-8577, Japan, sato.hisako.my@ehime-u.ac.jp*

† Footnotes relating to the title and/or authors should appear here.
Electronic Supplementary Information (ESI) available: [details of any supplementary information available should be included here]. See DOI: 10.1039/x0xx00000x

amyloids, peptides and proteins,[3,30–36] the low-molecular mass gelators could be synthesized artificially. Thus, the mirror-image relation between the antipodal pairs can be confirmed. It makes the phenomena more confident and reliable. We also provided the first example of the *in situ* monitoring of the build-up of stereoregular architects of molecules by the time-step VCD method. [73,82,85,89,90]

To strengthen the basis of the above-mentioned experimental efforts, an accurate large-scale simulation was performed for the vibrational properties of a model array of chiral molecules.[86] The simulation revealed the enhancement in VCD signals with an increase in the array length to a few hundred nanometres. The results presented a theoretical basis for rationalizing the enhancement of VCD signals for molecular aggregates.

In this perspective article, we report the opening of a new horizon for VCD spectroscopy by targeting gels, metal coordination compounds, and solid surfaces, all of which lead to remarkable signal enhancement. In the case of metal coordination compounds, VCD spectroscopy revealed the effect of spin multicity on their vibrational energy levels. The VCD band arising from the electronic transition to low-lying excited states was observed for a paramagnetic metal complex with $\Delta\Lambda$ isomerism. It was confirmed for the first time that the band satisfied the mirror-image relation between the optical antipodes. Regarding solid surfaces, we developed a solid-state VCD (SD-VCD) method to investigate intermolecular interactions. Stereoselective VCD enhancement was first observed on a solid surface, mainly caused by coherent vibration in a stacked pair. Finally, we describe an on-going project involving the construction of a multi-dimensional VCD system.

Criteria for VCD application for supramolecular chirality

Chiral low-molecular mass gelators are an example of supramolecular chirality generated through the spontaneous aggregation of small molecules.[102,103] A chiral gelator often leads to the formation of helical fibrils on a micrometre scale. The VCD method was employed to reveal how the molecular chirality of a gelator was amplified to the helicity of fibrils. When the work was started, there were rare reports on the application of the VCD method to gels. Therefore, to confirm the reliability of VCD signals, the observed spectra were validated as reflecting the true chiral vibrational properties of a molecule. Our criteria are as follows:

(i) The samples of antipodal molecules should have a mirror-image relation.

(ii) The samples containing a racemic mixture should not produce a VCD signal.

(iii) Linear dichroism (LD) is measured simultaneously to estimate its contribution to the observed signal. No inversion of signs is ascertained when a cell rotates around the direction of monitoring.

(iv) A corresponding IR peak should be obtained at the same wavenumber.

There is a possibility that a signal satisfying criteria (i)–(iii) appears due to physical reasons.[53] Such a signal, however, has no corresponding IR peak (criteria (iv)). The IR and VCD spectra were recorded using an assembled cell with CaF_2 windows and a Teflon spacer of 50 μm optical length. An isotropic solution containing a gelator at a concentration above the critical gel concentration was injected and cooled to room temperature. The final sample should be transparent as much as possible.[53] Once the signals satisfy the above criteria, analysis is proceeded according to the following steps:

(i) A large number of reliable VCD peaks are obtained because of signal enhancement.

(ii) The conformation of a gelator molecule is analysed in detail. In these procedures, the observed spectra are compared with the theoretical ones calculated for various conformations until the most probable conformation is obtained.

(iii) By connecting the molecules in the deduced conformation in reasonable manners, such as intermolecular hydrogen bonds, a model is constructed to show the organization of the molecules within a fibril.

Enhancement of VCD signals for gels: long-distance chiral transfer in 12-hydroxyhexadecanoic acid

VCD spectroscopy was first successfully applied to the benzene-d_6 (C_6D_6) gels of *R*- or *S*-12-hydroxyhexadecanoic acid (denoted as *R*-12-HOA or *S*-12-HOA, respectively).[76] The molecule is a chiral derivative of stearic acid with an asymmetric carbon atom at the 12th carbon position. The OH group attached to the 12th carbon atom is capable of forming a hydrogen bond with either the OH or the carboxyl group of another molecule, which leads to the formation of molecular networks.[102]

VCD spectra were so intense that they were obtained within a few hundred times of scanning. In contrast, no significant VCD signal was detected even after 10^4 accumulations for an isotropic CD_3OD solution containing the same amount of enantiomeric 12-HOA.

At first, the signal was suspected to be an artifact caused by linear dichroism arising from the crystalline domains in the gel. In spite of this suspicion, however, the observed signals satisfied criteria (i)–(iv), as stated in the previous section. The results indicated that the signals were true signals, which reflected the chiral properties of the composite molecule in the gel. The racemic mixture of 12-HOA did not form a gel in C_6D_6 but formed an isotropic solution with no VCD activity.[104]

For the C_6D_6 gels, distinct VCD peaks were observed in the wavenumber range of 1800–1000 cm^{-1}, where the vibrational peaks assigned to -COOH, -OH and -CH_2 appeared. All the peaks indicated a mirror-image relation between the antipodes in the wavenumber range of 1800–1000 cm^{-1}. The strong peaks at 1078 cm^{-1} (negative for *R*-12-HOA), 1130 cm^{-1} (positive), 1220

cm^{-1} (positive), 1271 cm^{-1} (positive), and 1437 cm^{-1} (positive) were related to the vibrations involving the asymmetric centre at carbon 12. In particular, a very strong couplet appeared, which was assigned to the C-O stretching of a carboxyl group. This is interesting because the planar carboxyl group is achiral. The results imply that the chiral nature of carbon 12 transferred to the carboxylic group through vibrational coupling along the long alkyl chain.

Another aspect was that the band for C=O stretching split into two components with opposite signs. This feature was ascribed to the formation of hydrogen bonds between the carboxylic groups. These analyses of the observed VCD signals were used to construct the model of molecular organization in a fibril. It consisted of a twisted dimer with intermolecular hydrogen bonding at the carbonyl groups (Figure 1). The proposed fibril model was quite different from the previous models and provided a clue to interpreting the gel properties by other researchers.[105]

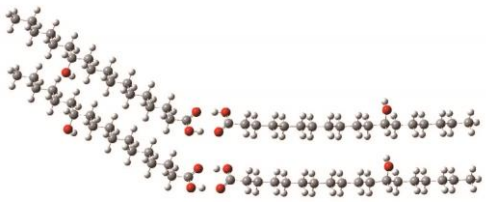

Figure 1. A model of molecular organization of *R*-12-HOA in a gel.

Perfluoroalkyl gelators: helical winding of perfluoro chains and temperature profiles

The VCD study was extended to the chiral low-molecular mass gelators with perfluoroalkyl chains. The compounds are particularly interesting for VCD application because the perfluoroalkyl chains wind helically due to the steric hindrance of the bulky fluorine atoms. Since the chain showed no electronic transition in the UV-vis region, ECD spectroscopy could not be applied to study the chiral properties of the chains. Before our investigation, Monde *et al.* studied the helical properties of a perfluoroalkyl chain in a solution by the means of VCD.[106]

The structures of the used compounds are shown in Chart 1. They are denoted as **CFn** (n = number of carbon atoms in the perfluoroalkanoyl chain; Chart 1). **CFn** possesses the head group of a cyclohexyl ring attached to two perfluoroalkanoyl chains through amide bonds. The molecule is capable of constructing a molecular array, forming two intermolecular hydrogen bonds at the amide groups in an anti-parallel way. The perfluoro chains are expected to reinforce such an array owing to their aggregative properties. The molecule was synthesized as a derivative of its alkanoyl analogue, which was first reported by Hanabusa *et al.* as an efficient gelator for a wide range of organic solvents.[103] **CFn**s were found to form a gel in several organic solvents such as acetonitrile, methanol, benzene, and C_6F_6.[78,79,83,84]

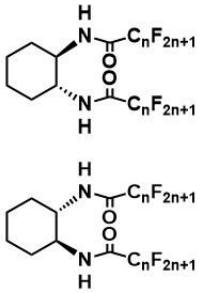

Chart 1. Molecular structures of *RR*-CFn (upper) and *SS*-CFn (lower). CF4, CF7, CF8, and CF9 correspond to compounds with n =3, 6, 7, and 8, respectively.

The phase transition from an isotropic solution to a gel was monitored by measuring the VCD spectrum of a CD_3CN solution containing ***SS*-CF7**.[89] No VCD peak was detected when the sample formed an isotropic solution in the temperature range of 60°C to 45°C. When the temperature was decreased below the sol-gel transition temperature (or 45°C in this case), distinct VCD signals appeared. The results confirmed that the enhancement of VCD signals was associated with the occurrence of sol-gel transformation. In addition, it was noted that the IR peaks assigned to the C=O stretching vibrations red-shifted by ca. 30 cm^{-1} during the sol-gel transition. This indicated the formation of hydrogen bonds at C=O and NH.

The VCD spectra of the gels formed by a series of **CFn**s (**n** = 7, 8, and 9; Chart 1) were recorded.[82–84] Table 1 summarizes the results focusing on the couplet peaks assigned to the C=O stretching vibrations. The splitting of the original peak was caused by intermolecular hydrogen bonding. For CD_3CN solvent, the enantiopure **CF7** and **CF9** yielded gels, while **CF8** did not. It was noted that the couplets of **CF7** and **CF9** had opposite signs**.** SEM analysis of the CH_3CN gels revealed that the fibrils of **CF7** and **CF9** were wound with opposite helicity. These results presented an example of chiral hierarchy showing how the molecular chirality was amplified to macroscopic scales. Furthermore, the sign of the couplet of the **CF7** gel inversed when the solvent was changed from CD_3CN to C_6F_6. The sign inversion was also observed for the **CF9** gels. The results indicated that the helical stability of a molecular array was significantly affected by the participation of solvent molecules (Figures 2(a) and (b)).

Figure 2(a) shows the VCD and IR spectra of the CD_3CN gels of ***RR*- and *SS*- CF7**s. The multiple peaks in the region of 1238–1170 cm^{-1} were assigned to the stretching vibrations of the C-F bonds in the perfluoroalkyl chains (denoted as PFCs).[78] The observed spectra were compared with the theoretical spectra calculated for a single molecule under various conformations. From the comparative analysis, it was deduced

that the PFCs were helical with right- or left-winding for ***RR*-CF7** and ***SS*-CF7**, respectively. The SEM images of the gels showed that the fibril is a right- or left-handed helical ribbon for ***RR*-CF7** or ***SS*-CF7**, respectively. Thus, the chirality of a fibril at the micrometre scale is uniquely related to the molecular chirality of the gelator.

The crystal structures of ***RR*-CF4** (n=3) and ***RR*-CF8** (n=7) were studied by single crystal X-ray or powder X-ray diffraction analysis.[83,87] ***RR*-CF4** was so packed as to form a molecular array with its cyclohexyl rings stacked parallel. In the array, the molecules were connected by two anti-parallel intermolecular hydrogen bonds at C=O and NH groups. The structure was consistent with the model proposed for the formation of a fibril. In the case of ***RR*-CF8**, the powder X-ray diffraction analysis revealed that an oxygen atom of one of the carbonyl groups in ***RR*-CF8** was free of hydrogen bonds.[85] In addition, one of the PFCs was a mixture of right- (*P*) and left-handed (*M*) helices, while the other was a purely *P* helix. The crystal structure analysis of ***RR*-CF8** revealed that the two amide groups formed hydrogen-bonded 1-D chains in parallel. The low gelation ability of chiral **CF8** in an organic solvent was related to the structural instability or the formation of only a single hydrogen bond in the connecting molecules.

The simulation of VCD spectra based on the structure determined by the above X-ray analyses, however, was unable to reproduce precisely the observed spectra of **CF7** and **CF8** in C_6F_6 solvent (Table 1). To reproduce the VCD signal of the gels of chiral **CF8** or **CF7** in C_6F_6, one possible model was introduced in which one of the perfluorinated chains adopted a bent conformation due to the cis-configuration at the β-carbon of the C=O group. Under the conformation, a pair of NH and C=O groups on different perfluorinated chains was positioned close enough to form an *intramolecular* hydrogen bond. The remaining pair of NH and C=O groups formed an intermolecular hydrogen bond with their adjacent molecules. A detailed large-scale simulation is required to confirm the validity of this model.

Time-step VCD measurements

The high intensity of the VCD signals indicated that sufficiently reliable signals were obtained with a small number of scans (< 100). One consequence was that it enabled the *in situ* monitoring of the structural development of a gel under various conditions such as temperature change, mixed solvents, or mixing of two different kinds of gelators.[82,85,89]

The time course of gel formation was monitored by VCD spectrum for an acetonitrile solution containing 0.012 mol L^{-1} ***RR*-CF7**. The concentration was chosen to be slightly above the critical gel concentration. Such a low concentration of the gelator resulted in a remarkable decrease in the gelation rate.[85,86] Immediately after the appearance of a gel, the ratio of the VCD to IR peak intensities (denoted as VCD/IR) for the peak arising from C=O stretching was determined as a function of time (Figure 3). It was found that the VCD/IR ratio continued to increase even after the onset of gelation until it reached a constant value after several minutes. This implied that the initially formed gel underwent further structural changes with time. One possibility was that the process involved the elongation of a gel fibril by the stripping of the CD_3CN molecules solvating the amide groups of the gelator through weak hydrogen bonds. It has been suggested that the average persistence length of molecular arrays is limited by the defects caused by thermal fluctuations and/or interactions with solvents. In the above examples, the rate of sol-gel transformation was controlled by selecting appropriate concentrations, gelators, and solvents for the required purposes. Compared with the synthetic materials used here, such adjustments are difficult for natural materials such as amyloids.

Table 1. Signs of C-O couplets in acetonitrile and C_6F_6 solvents

Gelator	Signs of C=O couplets in CD_3CN gels Low/high wavenumber	Helicity in acetonitrile gels by SEM	Signs of C=O couplets in C_6F_6 gels Low/high wavenumber	Morphology of C_6F_6 gels observed by SEM
***RR*-CF7** (n=6)	-/+	Right-handed helical ribbon or twisted fibril	+/-	Plate-like
***RR*-CF8** (n=7)	No gelation in chiral form, racemic form made gel	-	+/-	Fibril
***RR*-CF9** (n=8)	+/-	Left-handed helical ribbon	-/+	Fibril and tape

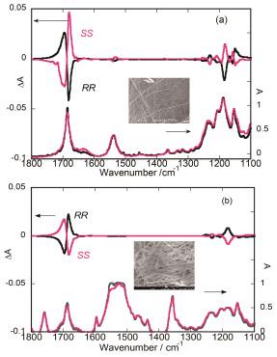

Figure 2. VCD and IR spectra of ***RR*-CF7** (black) and ***SS*-CF7** (red) in CD_3CN (a) and C_6F_6 gels (b). (Insets) SEM images of ***SS*-CF7** (modified from Ref. 78 and 82).

The observed enhancement in the VCD spectra during gel formation was compared with that in the theoretical spectra. [86]

For this purpose, the model of a helical chain was assumed in which enantiopure ***RR*-CF2** molecules were connected through two anti-parallel hydrogen-bonded chains at the amide groups. The number of molecules (N) was varied from 1 to 200 (denoted as (***RR*-CF2**)$_N$). The VCD/IR ratio, calculated as a function of the array length (N), increased monotonously with an increase in N until N reached ca. 100 (corresponding to ca. 50 nm length). Upon the formation of (***RR*-CF2**)$_N$ aggregates, intermolecular hydrogen bonds are formed between the secondary amide groups (O=C–N–H). There are two secondary amide groups in each ***RR*-CF2** molecule, and both of them are involved in intermolecular hydrogen bonding to form stable (***RR*-CF2**)$_N$ aggregates. As a result, a co-axial anti-parallel right-handed double helical structure is formed by the secondary amide groups. The chirality at the molecular scale is amplified in this way. The IR and VCD spectra of the C=O stretching mode calculated for the (***RR*-CF2**)$_{150}$ aggregate reproduced the couplet sign observed experimentally as shown in Figure 2(a).

The intensity of a VCD peak is given by the rotational strength, which is the dot product of the electric dipole transition moment and magnetic dipole transition moment. The main reason for the monotonous increase in rotational strength is that the contribution of intermolecular vibrational coupling to the magnetic transition moment did not decay with increasing N. This happened when the molecules were arranged regularly under a uniform conformation along a helical chain. On the contrary, the dipole transition moment, which was responsible for the IR intensity, had little contribution from the vibrational coupling between two molecules separated by a distance of 10 nm.

In gels, three tiers of chirality exist hierarchically: (i) the molecular chirality of the gelator, (ii) the co-axial anti-parallel right-handed double helical structure persistently continuing the ca. 50 nm length scale, and (iii) the helically wound fibrils extending to a few micrometres. The above theoretical simulation reveals that it is the second tier of chirality that causes the enhancement of VCD peaks.

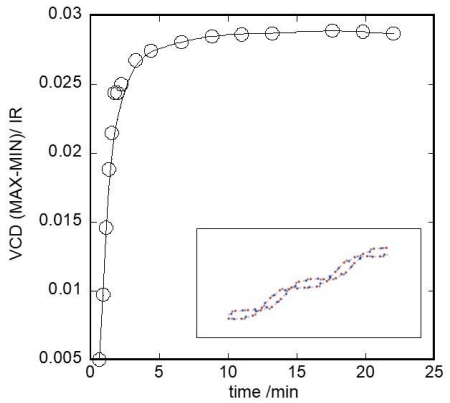

Figure 3. Change in the ratio of the relative intensities of VCD and IR peaks assigned to C=O stretching with time for ***RR*-CF7** in CD_3CN. (Inset) Model of a helical fibril (modified from Ref. 86).

The dynamic process of gelation can be followed in several ways (e.g., visual observation, light scattering, viscosity, and spectroscopic analyses such as IR, UV-vis, ECD, and NMR spectroscopies). Compared with these methods, the signal enhancement in VCD spectroscopy directly represents the build-up of the stereoregular molecular array of the gelator molecules. In other words, it evidences the construction of a well-organized molecular architecture at a scale of few hundred nanometres during the observation period (or within several minutes). In this respect, this was the first attempt at the *in situ* monitoring of a regular molecular organization, not a randomly oriented aggregation of molecule.

Enhancement of VCD signals in metal coordination

The chelation of a metal ion may result in the enhancement of VCD signals. [14,15] This effect was also noted by our group from the very beginning of the investigation.[16] The enhancement of VCD signals revealed the novel properties of metal complexes such as (i) the need for anharmonicity corrections of a metal complex with spins and (ii) the presence of low-lying excited states of a metal complex with spins. These were difficult to study by other spectroscopic methods.[18,19,68]

The experiments were mostly concerned with a series of [M(III)(acac)$_3$] (M= Co, Cr, and Ru; acac = acetylacetonato): [Co(III)(acac)$_3$] (d^6; S = 0), [Cr(III)(acac)$_3$] (d^3; S = 3/2,) and [Ru(III)(acac)$_3$] (d^5; S = 1/2). They possessed coordination chirality due to $\Delta\Lambda$ configurations. Figure 4 shows the VCD spectra in the wavenumber range of 1100–1700 cm^{-1}. The $\Delta\Lambda$ pairs showed a clear mirror-image relationship. The intensities of the VCD peaks were very high, e.g., $\Delta\varepsilon$ = 5 for chiral [Ru(III)(acac)$_3$].

Regarding the anharmonicity corrections of metal complex with spins, the signs of the couplet peaks assigned to the couplet vibrations of C=O/C-C around 1400 cm^{-1} were noted to be opposite for the Co(III) and Cr(III) complexes even for the same enantiomers. When theoretical calculations were performed within the harmonic approximation, the observed VCD spectra were well reproduced for [Co(III)(acac)$_3$]. On the contrary, the calculation at the same level of approximation failed to predict the observed spectra for [Cr(III)(acac)$_3$]. This was because of the difference in their spin-multiplicities. When the anharmonic effects were taken into account, the calculation reproduced the observed spectra of [Cr(III)(acac)$_3$] well. The results showed that the positions of the two peaks that appeared around 1400 cm^{-1}, which were assigned to the stretching vibrations of two C=O/C-C bonds, were predicted precisely together with their signs. Their relative positions were inverse to those of [Co(III)(acac)$_3$].[19]

Regarding the low-lying excited states of metal complex with spins, the spectra of chiral [Ru(III)(acac)$_3$] showed a large broad band in the wavenumber region of 1600 – 2500 cm^{-1}.[19] The bands exhibited the mirror-image relation between the Δ- and Λ-enantiomers. Time-dependent density functional calculation predicted the presence of the low-lying excited

states for this complex. The open-shell density functional theory calculation with MO6 exchange functional and all-electron Douglas-Kroll second order scalar relativistic correction could reproduce well other sharp VCD peaks observed in the range of 1100 – 1600 cm^{-1}.

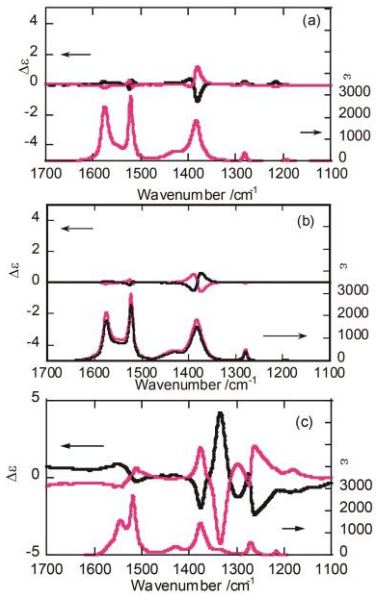

Figure 4. Observed IR and VCD spectra: (a) [Co(III)(acac)$_3$], (b) [Cr(III)(acac)$_3$], (c) [Ru(III)(acac)$_3$]. The black and red profiles are Λ and Δ, respectively (modified from Ref. 16, 18, and 19).

Solid-state VCD for intercalation compounds: stereoselective VCD enhancements

To investigate the intermolecular interaction on a solid surface, we developed the solid-state vibrational circular dichroism (SD-VCD).[92-98] The method was applied to inorganic intercalation compounds.[99-101] Here an attention was focussed on how VCD spectra were affected by the chirality relation between two different adsorbed species.[99]

Sodium montmorillonite was chosen as a host. [99,100,107] In montmorillonite, one layer is approximately 1 nm thick and negatively charged, and cationic species are intercalated in the interlayer spaces.[107] When montmorillonite is ion-exchanged with Δ- or Λ-$[Ru(phen)_3]^{2+}$ (phen = 1,10-phenanthroline), the resultant adduct exhibits a high selectivity towards the adsorption of chiral organic molecules such as *R*- or *S*-1,1'-bi-2-binaphthol (denoted as *R*-BINOL or *S*-BINOL, respectively). Chromatographic results showed that *R*-BINOL (or *S*-BINOL) was adsorbed more strongly than *S*-BINOL (or *R*-BINOL) on a clay surface modified with Δ-$[Ru(phen)_3]^{2+}$ (or Λ-$[Ru(phen)_3]^{2+}$). SD-VCD measurements were performed for montmorillonite samples co-adsorbing Δ- or Λ-$[Ru(phen)_3]^{2+}$ and *R- or S*-BINOL.

According to the simulation based on molecular association, a compact associate was formed for *R*-BINOL/Δ-$[Ru(phen)_3]^{2+}$ and *S*-BINOL/Λ-$[Ru(phen)_3]^{2+}$ (denoted as a strongly interacting pair), while a loose pair was formed for *R*-BINOL/Λ-$[Ru(phen)_3]^{2+}$ and *S*-BINOL/Δ-$[Ru(phen)_3]^{2+}$ (denoted as a weakly interacting pair) (Figure 5). The simulation was consistent with the experimentally observed chromatographic results.

The observed VCD spectra, which reflect the chirality relation, of the strongly and weakly interacting pairs differed significantly. Notably, in the wavenumber region where the IR bands of the co-adsorbed species were partially overlapped, the signals enhanced stereoselectively. In other words, the VCD peak assigned to chiral BINOL enhanced for the strongly interacting pair, while no such enhancement was observed for the weakly interacting pair. In such a region, both of them could be excited vibrationally. In fact, upon scrutinizing their motions in the model, both the components were found to move in a coherent way for the strongly interacting pair, whereas each component moved independently for the weakly interacting pairs.

Based on these results, it was postulated that the delocalization of vibrational motions in a compactly associating pair resulted in the enhancement of the VCD peak assigned to either of the components. IR spectroscopy is extensively employed to identify the reaction intermediates in heterogeneous catalysis.[108] The '*stereoselective VCD enhancement*' observed here could provide a clue to investigating the intermolecular interaction within a solid or on a solid surface.

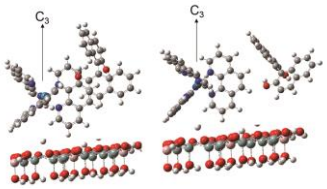

Figure 5. Schematic images of *R*-BINOL /Δ-$[Ru(phen)_3]^{2+}$ (strongly interacting pair) (left) and *R*-BINOL /Λ-$[Ru(phen)_3]^{2+}$(weakly interacting pair)(right).

Future work

In terms of instrumental improvement, our VCD system was combined with a reflection-absorption spectrometer for the first time in collaboration with JASCO Corporation (Japan) (named as PRESTO-S-2007). The instrument has now been updated with the provision of simultaneous measurement of linear dichroism (named as PRESTO-S-2016 (VCD/LD)).

We are now developing a multi-dimensional VCD system, in which 'time' and 'position' are added as additional axes. For this purpose, an instrument with a quantum cascade laser (1500–1740 cm^{-1}) is being constructed in collaboration with JASCO Corporation (Japan) (named as MDVCD-MIRAI-2020). Figure 6 shows one of the preliminary results. Here, a distinct

VCD peak is obtained for a CH_2Cl_2 sample containing Fmoc-L- or -D-Leucine with an absorbance as high as 4. The spectra were recorded by scanning in the wavenumber range of a resolution of 0.5 cm^{-1}. The time required for measurement at each wavenumber was less than 1 s.

It is now moving to the next stage, in which a system with a high spatial resolution will make it possible to scan the VCD activity at a micrometre scale. The instrument will be used to analyse the DL effects on the aggregative properties of biopolymers such as an amyloid containing D-amino acid residues.

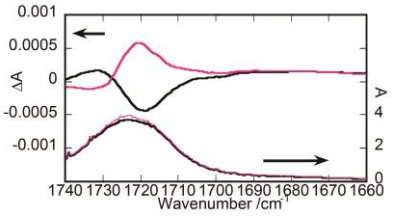

Figure 6. Examples of IR (lower) and VCD (upper) spectra of Fmoc-L-Leucine (black) and Fmoc-D-Leucine (red) in CH_2Cl_2 obtained using QCL laser instruments. The path length of the liquid cell was 2 mm, and the concentration was 7.12 mg mL^{-1}.

Conclusions and Outlook

We described the VCD method applied to supramolecular systems. The development of solid state and time-step VCD methods opened a new horizon in determining the mechanism of chirality amplification from the microscopic to supramolecular scales. The VCD signals enhanced in the following three cases: (i) chiral gels with hundreds of molecules arranged in stereoregularly, (ii) chiral metal complexes with low-lying excited states in the IR region, and (iii) a molecular pair interacting stereoselectively on a solid surface.

A project on the construction of a multi-dimensional VCD system using QCL as an IR light source was described. Highly dense aqueous samples such as blood, serum, and peptide could be the targets for this system.

Conflicts of interest

There are no conflicts to declare.

Acknowledgements

The author appreciates Dr. Akihiko Yamagishi (Toho University) for invariable discussions. The author thanks the late Prof. Kayako Hori, Prof. Tomoko Yajima (Ochanomizu University), Prof. Hirotoshi Mori (Chou University), Prof. Hajime Torii (Shizuoka University), Prof. Izuru Kawamura (Yokohama National University), Prof. Jun Yoshida (Kitasato University), and Mr. Jun Koshoubu (JASCO Corporation) for variable collaboration. This work was supported by Grants-in-Aid for Scientific Research from the Ministry of Culture, Sports, Science and Technology of Japan (JP17H03044) and JST MIRAI grants (JPMJMI18GC). The computations were performed at the Research Center for Computational Science, Okazaki, Japan.

Notes and references

1 L. A. Nafie, *Vibriational optical activity: Principles and Application*s, Wiley, Chichester, 2011.
2 P. J. Stephens, F. J. Devlin and J. R. Cheeseman, *VCD Spectroscopy for Organic Chemists*, CRC Press, Florida, 2012.
3 T. A. Keiderling, *Molecules*, 2018, **23**, 2404. DOI:10.3390/molecules23092404; T. M. Keiderling, *Chem. Rev.*, 2020, DOI:10.1021/acs/chemrev.9b00636.
4 P. L. Polavarapu, *Vibrational Spectra: Principles and Applications with emphasis of optical activity*, Elsevier, The Netherlands, 1998.
5 T. A. Keiderling and A. Lakhani, *Chirality*, 2018, 1, doi.org/10.1002/chir.22799.
6 S. Abbate, G. Longhi, G. Mazzeo, C. Villani, S. Petković§ and R. Ruzziconi*, RSC. Adv.*, 2019, **8**, 11781.
7 P. J. Stephens, *J. Phys. Chem.,* 1985, **89**, 748.
8 G. Holzwarth, E. C. Hsu, H. S. Mosher, T. R. Faulkner and A. Moscowitz, *J. Am. Chem. Soc.,* 1974, **96**, 251.
9 L. A. Nafie, T. A. Keiderling and P. J. Stephens, *J. Am. Chem. Soc.,* 1976, **98**, 2715; L. A. Nafie, *Chirality*, 2020, 1-26, DOI:10.1002/chir.23191.
10 J. Sadlej, J. C. Dobrowolski and J. E. Rode, *Chem. Soc. Rev.,* 2010, **39**, 1478.
11 T. Wu, X.-Z. You and P. Bouř, *Coord. Chem. Rev.*, 2015, **284**, 1.
12 H. Sato, A. Yamagishi, *International Journal of Molecular Sciences,* 2013, **14**, 964.
13 W. Dzwolak, *Chirality*, **2014**, 26, 580.
14 Y. He, X. Cao, L. A. Nafie and T. B. Freedman, *J. Am. Chem. Soc.* 2001, **123**, 11320.
15 L. A. Nafie, *J. Phys. Chem. A,* 2004, **108***,* 7222.
16 H. Sato, T. Taniguchi, K. Monde, S.-I. Nishimura and A. Yamagishi, *Chem. Lett.*, 2006, **35**, 364.
17 C. Johannessen and P. W. Thulstrup, *Dalton Trans.*, 2007, 1028.
18 H. Sato, T. Taniguchi, A. Nakahashi, K. Monde and A. Yamagishi, *Inorg. Chem.* 2007, **46**, 6755.
19 H. Mori, A. Yamagishi and H. Sato*, J. Chem. Phys.,* 2011, **135**, 084506.
20 S. R. Domingos, A, Huerta-Viga, L. Baij, S. Amirjalayer, D. A. E. Dunnebier, A. J. C. Walters, M. Finger, L. A. Nafie, B.de Bruin, W. J. Buma and S. Woutersen, *J. Am. Chem. Soc.*, 2014, **136**, 3530.
21 S. R. Domingos, H. J. Sanders, F. Hartl, W. J. Buma and S. Woutersen, *Angew. Chem. Int. Ed.*, 2014, **53**, 14042.
22 S. R. Domingos, F. Hartl, W. J. Brma and S. Woutersen, *ChemPhysChem,* 2015, **16**, 3363.
23 Z. Dezhahang, M. R. Poopari, J. Cheramy and Y. Xu, *Inorg. Chem.*, 2015, **54**, 4539.
24 Z. Dezhahang, M. R. Poopari, F. E. Hernandez, C. Diaz and Y. Xu, *Phys. Chem. Phys. Chem.*, 2014, **16**,12959.
25 C. Merten, M. Robert and Y. Xu, *Inorg. Chem*., 2014, **53**, 3177.
26 C. Merten, K. Hiller and Y. Xu, *Phys. Chem. Phys. Chem.*, 2012, **14**, 12884.
27 H. Miyake, K. Terada and H. Tsukube, *Chirality*, 2014, **26**, 293.
28 G. Szilvágyi, B. Brém, G. Báti, L. Tölgyesi, M. Hollósi and E. Vass, *Dalton Trans.*, 2013, **42**, 13137.

29 G. Pescitelli, S. Lüdeke, M. Coórecki and L. Di Bari, *J. Phys. Chem. Lett.*, 2019, **10**, 650.
30 A. Fulara, A. Lakhani, S. Wójcik, H. Nieznańska, T. A. Keiderling and W. Dzwolak, *J. Phys. Chem. B,* 2011, **115**, 11010.
31 D. Kurouski, R. A. Lombardi, R. K. Dukor, I. K. Lednev and L. A. Nafie, *Chem. Commun.,* 2010, **46**, 7154.
32 D. Kurouski, R. K. Dukor, X. Lu, L. A. Nafie and I. K. Lednev, *Chem. Commun.*, 2012, **48**, 2837.
33 A. Giugliarelli, P. Sassi, M. Paolantoni, A. Morresi, R. Dukor and L. A. Nafie, *J. Phys. Chem. B*, 2013, **117**, 2645.
34 D. Kurouski, X. Lu, L. Popova, W. Wan, M. Shanmugasundaram, G. Stubbs, R. K. Dukor, I. K. Lednev and L. A. Nafie, *J. Am. Chem. Soc.*, 2014, **136**, 2302.
35 M. Pazderková, T. Pazderka, M. Shanmugasundaram, R. K. Dukor, I. K. Lednev and L. A. Nafie, *Chirality*, 2017, **29**, 469.
36 W. R. W. Welch, J. Kubelka and T. A. Keiderling, *J. Phys. Chem. B*, 2013, **117**, 10343.
37 J. Průša and P. Bouř, *Chirality*, 2018, **30**, 55.
38 A. G. Petrovic and P. L. Polavarapu, *J. Phys. Chem. B,* 2005, **109**, 23698.
39 G. Shanmugam, P. L. Polavarpu, E. Láng and Z. Maje, *J. Struct. Biol.*, 2012, **177**, 621.
40 H. Sato, T. Yajima and A. Yamagishi, *Chirality*, 2015, **27**, 659.
41 B. Martial, T. Lefèvre, T. Buffeteau and M. Auger, *ACS Nano,* 2019, **13**, 3232.
42 B. Nieto-Ortega, V. J. Nebot, J. F. Miravet, B. Escuder, J. T. L. Navarrete, J. Casado and F. J. Ramírez, *J. Phys. Chem. Lett.*, 2012, **3**, 2120.
43 F. Aparicio, B. Nieto-Ortega, F. Nájera, F. J. F. J. Ramírez, J. T. L. Navarrete, J. Casado and L. Sánchez, *Angew. Chem. Int. Ed.*, 2014, **53**, 1373.
44 R. Marty, H. Frauenrath and J. Helbing, *J. Phys. Chem. B*, 2014, **118**, 11152.
45 N. V. Ilawe, R. Schweitzer-Stenner, D. DiGuiseppi and B. M. Wong, *Phys. Chem. Chem. Phys.,* 2018, **20**, 18158.
46 T. J. Measey, K. B. Smith, S. M. Decatur, L. Zhao, G. Yang and R. Schweitzer-Stenner, *J. Am. Chem. Soc.,* 2009, **131**, 18218.
47 T. J. Measey and R. Schweitzer-Stenner, *J. Am. Chem. Soc.,* 2011, **133**, 1066.
48 C. Merten, *Phys. Chem. Phys. Chem.*, 2017, **19**, 18803.
49 S. Jähnigen, A. Scherrer, R. Vuilleumier and D. Sebastiani, *Angew. Chem. Int. Ed.,* 2018, **57**, 13344.
50 R. Knipper, T. G. Mayerhöfer, V. Kopecký, Jr., U. Huebner and J. Popp, *ACS Photonics*, 2018, **5**, 1176.
51 R. Knipper, V. Kopecký, Jr., U. Huebner, J. Popp and T. G. Mayerhöfer, *ACS Photonics,* 2018, **5**, 3238.
52 B. Nieto-Ortega, F. Garcia, G. Longhi, E. Castiglioni, J. Calbo, S. Abbate, J. T. L. Navarrete, F. J. Ramíre, E. Ortí, L. Sánchez and J. Casado, *Chem. Commun.,* 2015, **51**, 9781.
53 P. Rizzo, S. Abbate, G. Longhi and G. Guerra, *Opt. Mater.*, 2017, **73**, 595.
54 M. Bieri, C. Gauter and T. Bürgi, *Phys. Chem. Phys. Chem.*, 2007, **9**, 671.
55 S. R. Bhattacharya and T. Bürgi, *Nanoscale*, 2019, **11**, 23226.
56 A. Sels, R. Azoulay, W. J. Buma, M. A. J. Koenis, V. P. Nicu and T. Bürgi, *J. Phys. Chem. C*, 2019, **123**, 22586.
57 B. H. Strudwick, M. A. J. Koenis, H. J. Sanders, V. P. Nic, S. Woutersen and W. J. Buma, *Chem. Eur. J.* , 2019, **25**, 12560.
58 S. Lüdeke, M. Pfeifer and P. Fischer, *J. Am. Chem. Soc.*, 2011, **133**, 5704.
59 A. Rüther, M. Pfeifer, V. A. Lórenz-Fonfría and S. Lüdeke, *J. Phys. Chem. B,* 2014, **118**, 3941.
60 A. Lambrecht, M. Pfeifer, W. Konz, J. Herbst and F. Axtmann, *Analyst,* 2014, **139**, 2070.
61 J. Helbing and M. Bonmarin, *Chimia*, 2009, **63**, 128.
62 H. Rhee Y. G. June, J. S. Lee, K.K. Lee, J. H. Ha, Z. H. Kim, S. J. Jeon and M. Cho, *Nature,* 2009, **458**, 310.
63 X. Lu, H. Li, J. W. Nafie, T. Pazderka, M. Pazderková, R. K. Dukor and L. A. Nafie, *Applied Spectroscopy*, 2017, **71**, 1117.
64 H. Sato, Y. Mori, Y. Fukuda and A. Yamagishi, *Inorg. Chem.,* 2009*,* **48***,* 4354.
65 H. Sato, D. Shirotani, K. Yamanari and S. Kaizaki, *Inorg. Chem.,* 2010*,* **49**, 356.
66 H. Sato, H. Uno and H. Nakano, *Dalton Trans.*, 2011, **40**, 1332.
67 H. Sato, R. Takase, Y. Mori and A. Yamagishi, *Dalton Trans.*, 2012, **41**, 747.
68 H. Sato, F. Sato, M. Taniguchi and A. Yamagishi, *Dalton Trans.*, 2012, **41**, 1709.
69 H. Sato, Y. Mori, T. Kitazawa and A. Yamagishi, *Dalton Trans.*, 2013, **42**, 232.
70 H. Sato, Y. Mori and A. Yamagishi, *Dalton Trans.*, 2013, **42**, 6873.
71 S. Kaizaki, D. Shirotani and H. Sato, *Phys. Chem. Chem. Phys*., 2013, **15**, 9513.
72 K. Takimoto, Y. Watanabe, S. Mori and H. Sato*, Dalton. Trans*., 2017, **46**, 4397.
73 H. Sato, F. Sato and A. Yamagishi, *Inorganics*, 2018, **6**, 70.
74 Y. Goto, Y. Watanabe, A. Noboriguchi, J. Yoshida, S. Mori and H. Sato, *Dalton. Trans*., 2019, **48**, 10138.
75 S. Ishihara, J. Labuta, Z. Futera, S. Mori, H. Sato, K. Ariga and J. P. Hill, *J. Phys. Chem. B*, 2018, **122**, 5114.
76 H. Sato, K. Hori, T. Sakurai and A. Yamagishi, *Chem. Phys. Lett.*, 2008, **467**, 140.
77 H. Sato, T. Sakurai and A. Yamagishi, *Chem. Lett.*, 2011, **40**, 25.
78 H. Sato, T. Yajima and A. Yamagishi, *Chem. Commun.*, 2011, **47**, 3736.
79 K. Kohno, K. Morimoto, N. Manabe, T. Yajima and A. Yamagishi, *Chem. Commun.,* 2012, **48**, 3860.
80 H. Sato, T. Nakae, K. Morimoto and K. Tamura, *Org. Biomol. Chem.*, 2012, **10**, 1581.
81 H. Sato, E. Nogami, T. Yajima and A. Yamagishi, *RSC Adv*., 2014, **4**, 1659.
82 H. Sato, T.Yajima and A. Yamagishi, *RSC Adv.*, 2014, **4**, 25867.
83 T. Yajima, E. Tabuchi, E. Nogami, A. Yamagishi and H. Sato, *RSC Adv.*, 2015, **5**, 80542.
84 H. Sato, T. Yajima and A. Yamagishi, *Chirality*, 2016, **28**, 361.
85 H. Sato, T. Yajima and A. Yamagishi, *Phys. Chem. Chem. Phys.*, 2018, **20**, 3210.
86 H. Torii and H. Sato, *Phys. Chem. Chem. Phys.*, 2018, **20**, 14992.
87 T. Sasaki, A. Egami, T. Yajima, H. Uekusa and H. Sato, *Cryst. Growth Des.*, 2018, **18**, 4200.
88 H. Park, K. Y. Kim, S. H. Yung, Y. Choi, H. Sato and J. H. Jung, *Chem. Mater.,* 2018, **30**, 2074.
89 H. Sato, K. Watanabe and J. Koshoubu, *Chem. Lett.,* 2018, **47**, 1435.
90 T. Taniguchi, K. Monde, S. Nishimura, J. Yoshida, H. Sato and A. Yamagishi, *Mol. Cryst. Liq. Cryst.,* 2006, **460**, 107.
91 J. Yoshida, S. Tamura, K. Hoshino, H. Yuge, H. Sato, A. Yamazaki, S. Yoneda and G. Watanabe, *J. Phys. Chem. B*, 2018, **122**, 10615.
92 T. Sasaki, I. Hisaki, T. Miyano, N. Tohnai, K. Morimoto, H. Sato, S. Tsuzuki and K. Miyata, *Nat. Commun.*, 2013, **4**, 1787.
93 H. Sato, I. Kawamura, A. Yamagishi and F. Sato, *Chem. Lett.,* 2017, **46**, 449.
94 B. Mijiddorj, S. Kaneda, H. Sato, Y. Kitahashi, N. Javkhlantugs, A. Naito, K. Ueda and I. Kawamura, *BBA-Proteins and Proteomics*, 2018, **1866**, 789.
95 Y. Ozawa, H. Sato, Y. Kawano, N. Yamaki, Y. Izato, A. Miyake, A. Naito and I. Kawamura, *Phys. Chem. Chem. Phys.*, 2019, **21** 10879.
96 I. Kawamura and H. Sato, *Anal. Biochem.*, 2019, **580**, 14.
97 T. Sasaki, M. Miyata and H. Sato, *Cryst. Growth Des.,* 2018, **18**, 4621.
98 B. Mijiddorj, Y. Matsuo, H. Sato, K. Ueda and I. Kawamura, *Appl. Sci.*, 2019, **9**, 2601.

99 H. Sato, K. Tamura, K. Takimoto and A. Yamagishi, *Phys. Chem. Chem. Phys.*, 2018, **20**, 3141.
100 H. Sato, K. Takimoto and A. Yamagishi, *Phys. Chem. Chem. Phys.*, 2018, **20**, 25421.
101 H. Sato, K. Takimoto, I. Kawamura and S. Aisawa, *Bull. Chem. Soc. Jpn.*, 2019, **92**, 1779.
102 T. Tachibana, T. Mori and K. Hori, *Nature* 1979, **278**, 578.
103 K. Hanabusa, M. Yamada, M. Kimura and H. Shirai, *Angew. Chem. Int. Ed.,* 1996, **35**, 1949.
104 T. Sakurai, Y. Masuda, H. Sato, A. Yamagishi, H. Kawaji, T. Atake and K. Hori, *Bull. Chem. Soc. Jpn.*, 2010, **83**, 145.
105 S. Dieterich, T. Sottmann and F. Giesselmann, *Langmuir*, 2019, **35**, 16793.
106 K. Monde, N. Miura, M. Hashimoto, T. Taniguchi and T. Inabe, *J. Am. Chem. Soc.,* 2006, **128**, 6000.
107 A. Yamagishi and H. Sato, *Clays and Clay Miner.*, 2012, **60**, 411.
108 K. Tanaka, in *Dynamic Chemical Processes on Solid Surfaces*, Springer, Singapore, 2017, Chapter 10, 59-73.